47th AIAA/ASME/SAE/ASEE Joint Propulsion Conference & Exhibit
31 July - 03 August 2011, San Diego, California

AIAA 2011-5791

Space-time correlations and the Taylor hypothesis behind forced detonations

Luca Massa* and Monika Chauhan ,† and Frank K. Lu,‡
University of Texas at Arlington, Arlington, Texas, 76019

The competition between the intrinsic motion of detonation and convected disturbance is analyzed computationally by both performing a dynamic mode decomposition analysis and obtaining the space-time correlations. The dynamic modes are considerably affected by the presence of pre-shock forcing, while the space-time correlations are weakly affected by the convected turbulence. The triple point motion dominates the space-time correlations and manifests itself with a shift of the ellipsis towards the shock front.

I. Introduction

Rotating detonation engines (RDE) feature a non-uniform preshock field as a consequence of the filling process. The interface between mixed products from a previous wave and the fresh mixture supports a shear layer that impinges on the wave front as shown in Fig. 1. Such an interaction between convected vorticity and the detonation wave defines non-ideal propagating waves and is of practical importance because non-ideal detonations are characterized by a wave speed deficit and hot spots.[1] The effect of non-ideal preshock conditions on the performance of RDE is not known. In the previous work[2,3] we have shown that turbulence–detonation interaction can be analyzed from two points of view. First, the coupling between the exothermic structure of the detonation wave and the convected vorticity can be described in terms of the ratio between half reaction distance and Taylor microscale $N \equiv L_{1/2}/\lambda_0$, and leads to selective amplification of wave amplitudes in Fourier space. Second, the analysis of the interaction between convected preshock perturbation and self-excited structures points to the importance of freestream entropic fluctuations in changing the postshock statistics. The present paper analyzes the interaction between preshock vorticity and the front in terms of space-time correlations. The primary objective of the research is to understand the space-time coupling between lead shock and convected entropy and acoustic waves, thus space-time propagation of structures. This effort will lead to the development and validation of sub-grid models for the postshock field.

He et al.[4] analyzed isotropic flows and correlated the accuracy of large eddy simulation (LES) models to the prediction of both energy spectra and sweeping velocity. For shear (convectively unstable) flows, He and Zhang[5] proposed an elliptic model for time-space correlations that compounds information from both convective (i.e. associated with the Taylor hypothesis) and random sweeping velocity (i.e. associated with homogeneous turbulence with zero mean). In a recent work[3] we have shown that a detonation wave is an absolutely rather than convectively unstable system and its receptivity to postshock perturbations extends several half-reaction distances behind the lead front. The present paper aims to validate and extend elliptic models to the chemically reactive, self-excited post-detonation flow by determining contour of space-time cross correlations under entropic and vortical forcing. The focus is on the existence of a unique convection velocity, its scaling with the Chapman-Joguet (CJ) speed and the contribution of intrinsic scales. Cross-correlations are evaluated based on large scale three-dimensional Navier-Stokes simulations carried out with a high resolution WENO scheme. Correlation results at different distances from the lead shock are presented.

*Assistant Professor, Aerodynamics Research Center, Department of Mechanical and Aerospace Engineering. Senior Member AIAA.
†Graduate Student, Department of Mechanical and Aerospace Engineering.
‡Professor and Director, Aerodynamics Research Center, Department of Mechanical and Aerospace Engineering. Associate Fellow AIAA.

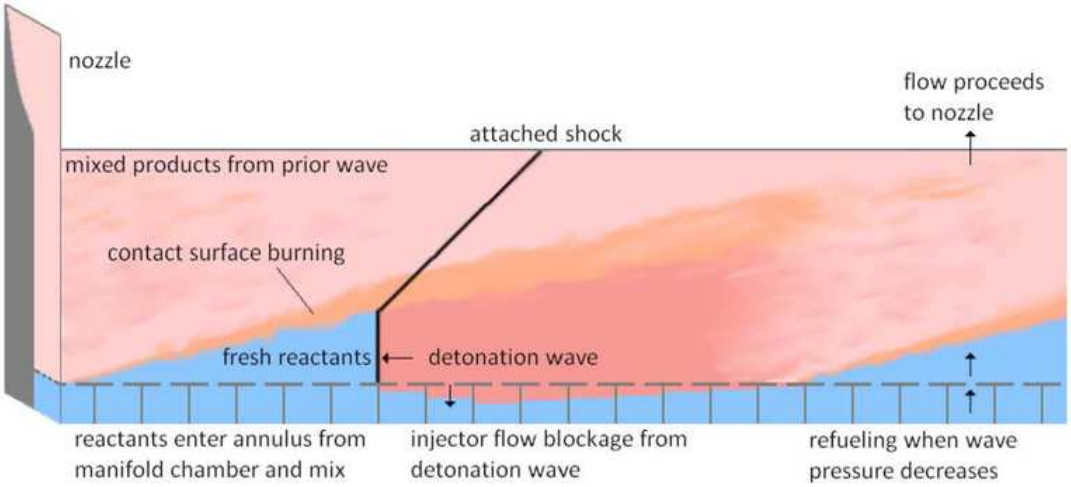

Figure 1. Schematic of filling process in a rotating detonation engine. The blue shaded area shows the fresh mixture, while the red shaded area shows the burnt mixture.

II. Methodology

A fifth-order WENO scheme with third-order Runge-Kutta time integration has been developed and validated against the linear growth rate of small perturbations in Chapman-Joguet detonations. The algorithm is applied here to obtain numerical solutions for three detonation cases: non-forced, vorticity-forced, and entropy-forced. The cases are illustrated in detail in Massa et al.[3] The magnitude of the vortical forcing is given by the pre-shock turbulent Mach number, $M_t = 0.235$. The entropic case is related to the vortical analog by the Morkovin's[6] form of the strong Reynolds analogy, which links density and velocity fluctuations in the pre-shock through $\frac{\rho'}{\bar{\rho}} = (\gamma - 1)M^2 \frac{u'}{\bar{u}}$.

The non-dimensionalization discussed in[3] leads to a set of parameters described below. For a CJ detonation, the heat release parameter Q is expressed in terms of the free-stream Mach number M as $Q \equiv \frac{\tilde{Q}}{p_0/\rho_0} = \frac{\gamma\left(M^2-1\right)^2}{2(\gamma^2-1)M^2}$.

A Mach number of 5.5 yields an adiabatic flame temperature of 2230 K, similar to that of small paraffins in stoichiometric air. The scaled activation energy is taken close to the longitudinal instability limit for planar detonations, with the rationale that galloping detonations feature slow pulsations that complicate the task of obtaining meaningful averages.[1] The Reynolds number based on the pre-shock Taylor scales is $Re_\lambda \equiv (\rho_0 u_{rms}\lambda)/(\mu_0) = 35$, the Prandtl and Lewis numbers are fixed $Pr = 0.72$ and $Le = 1$. The isentropic index is set to $\gamma = 1.2$ leading to a CJ velocity of $v_{cj} \approx 1800$m/s, in good agreement with methane/air and propane/air mixtures.[7] A final non-dimensional parameter expresses the ratio of Taylor microscale to half-reaction distance $L_{1/2}$, i.e., $N \equiv L_{1/2}/\lambda_0$.

Two values of N are used in previous work.[3] Small scale simulations where the transverse distance is smaller than the cell size are carried out with $N = 1$, and discussed in the dynamic mode decomposition section §III.A. A grid of size $500 \times 101 \times 101$ is used to simulate a domain with transverse extension $L_y = L_z = 9.1961\ L_{1/2}$. Larger simulations, where the transverse domain is multiple times the cell size, are carried out with a reduced value, $N = 0.3$, in order to properly resolve the convected turbulence. Large simulations are performed on meshes of size $550 \times 230 \times 230$ and domains with transverse extension $L_y = L_z = 82.4\ L_{1/2}$. We showed that the two sets of grids provide similar results, thus only small grid computations are discussed herein.

III. Elliptic model of space-time correlation

The streamwise velocity correlation behind the detonation wave is evaluated as

$$R\left(r, \tau; x_1\right) = \left\langle u_1\left(x_1 + r, x_2, x_3, t + \tau\right) u_1\left(x_1, x_2, x_3, t\right)\right\rangle. \tag{1}$$

Taylor's hypothesis, if valid, leads to linear contours of R in the $r,\ \tau$ plane, i.e.,

$$Rr, \tau; x_1 = \tilde{R}\left(r - U\tau, x_1\right), \tag{2}$$

for some function $\tilde{R}$. For shear flows, He and Zhang[5] have shown that constant correlation contours are ellipses centered on the origin. In the present case, the dispersion relation defined by the detonation instability problem cause the ellipsis to bend and shift away from the (0,0) point. In this section we analyze such contours and investigate the effect of boundary forcing. The reader should refer to our previous work on turbulence–detonation interaction[3] for a detailed explanation of the forcing conditions.

The contours of the space-time correlation for the three forcing cases are shown in Figs. 2-4. A comparison among the three figures demonstrates that the forcing affects the contours marginally. On the other hand, the streamwise non-homogeneity of the flow in the post-shock region supports elliptic profiles that are bent towards the $r-$axis. More importantly, the profiles shift towards the bottom as the distance from the shock increases. For large distances the shapes stabilize, but the purely advective condition of equation (2) is not recovered. In particular, the maximum correlation is not at the origin $(r, \tau) = (0, 0)$, but is shifted towards the shock and at $\tau = -0.5L_{1/2}/\sqrt{p_0/\rho_0}$, where the subscript 0 denotes the preshock, and $L_{1/2}$ is the half reaction distance. For an autocorrelation field, the outcome that the maximum is away from the origin might seem a surprising result. This is explained by the rationale that perturbations at the shock front are larger than in the burnt free-stream because they are supported by evanescent acoustic perturbations. Thus, we conclude that the contribution of evanescent acoustics sustained by the corrugating shock makes the Taylor's hypothesis invalid behind the detonation wave.

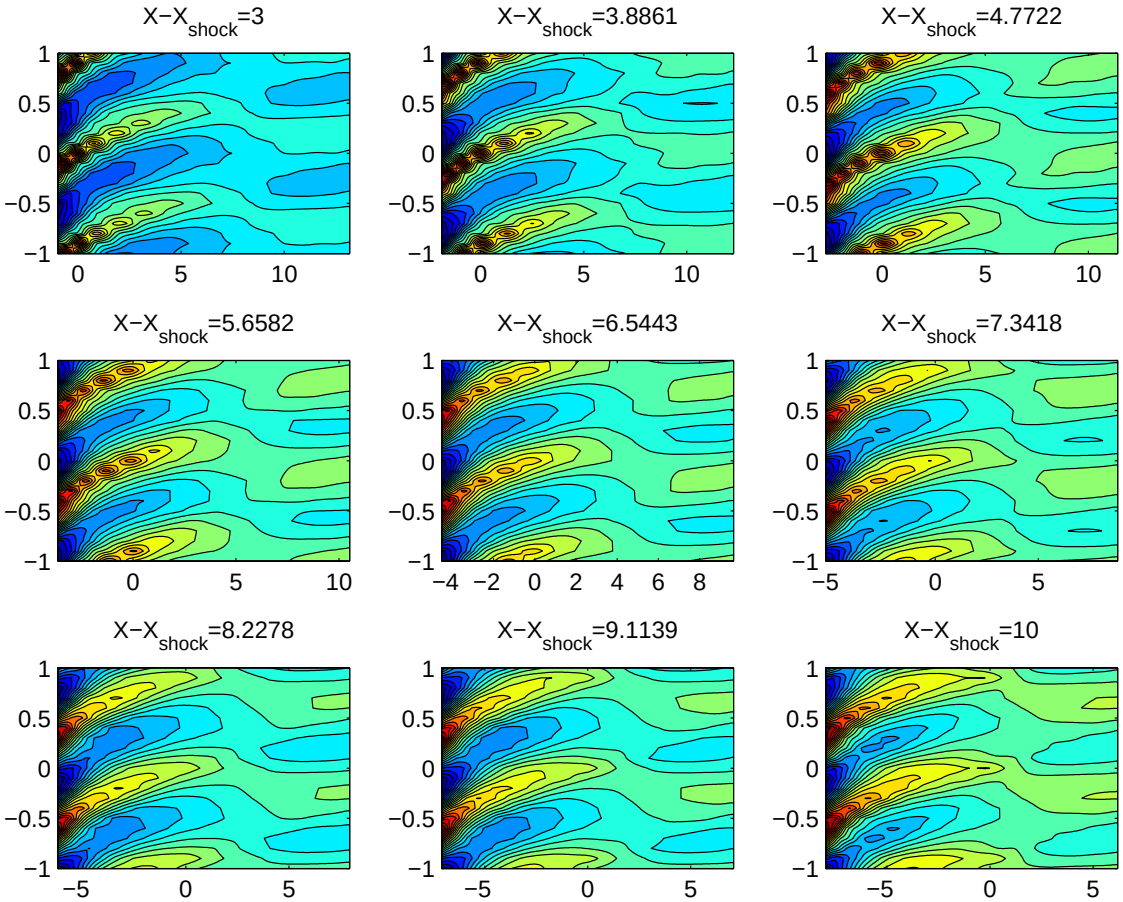

Figure 2. Non-Forced case space-time correlations versus r on the horizontal axis and τ on the vertical one. The panel heading reports the distance from the shock. Flow is from left to right.

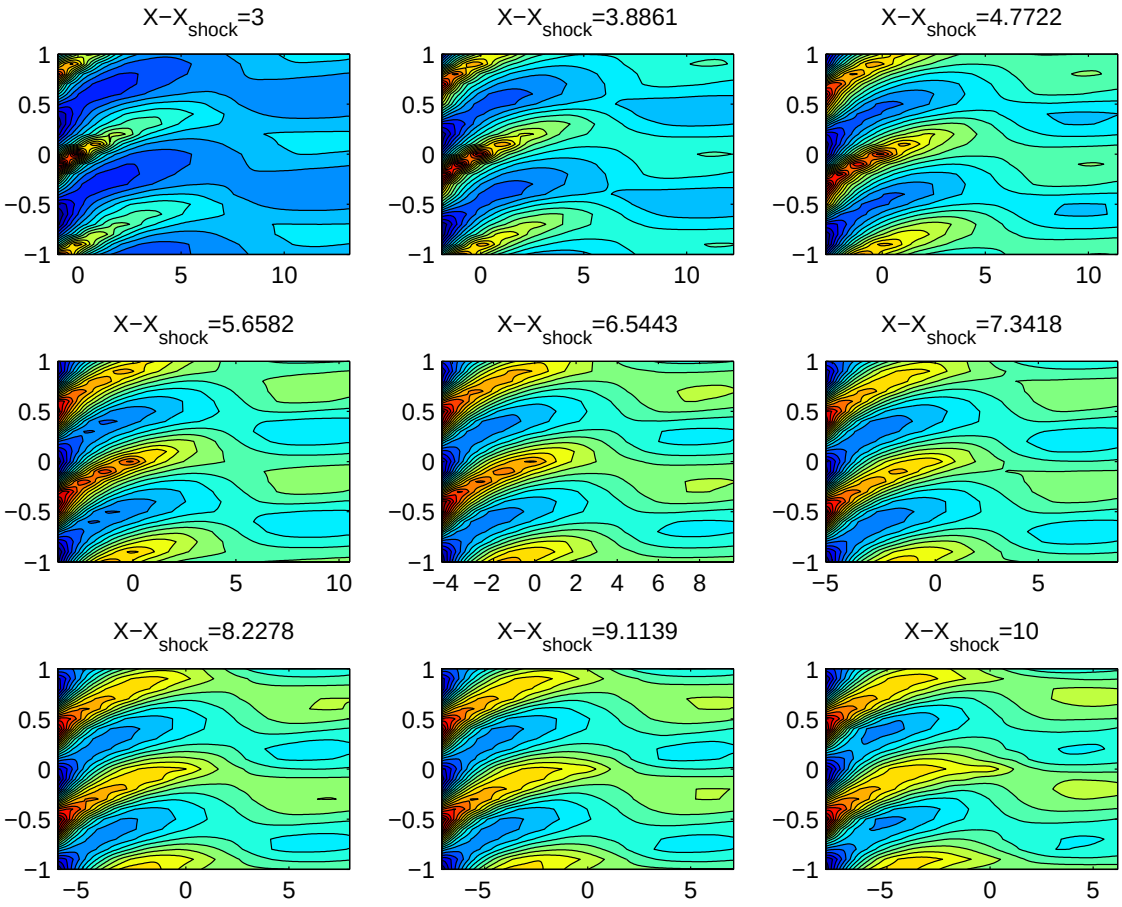

Figure 3. Similar layout as described in Fig. 2, but for vorticity forced case.

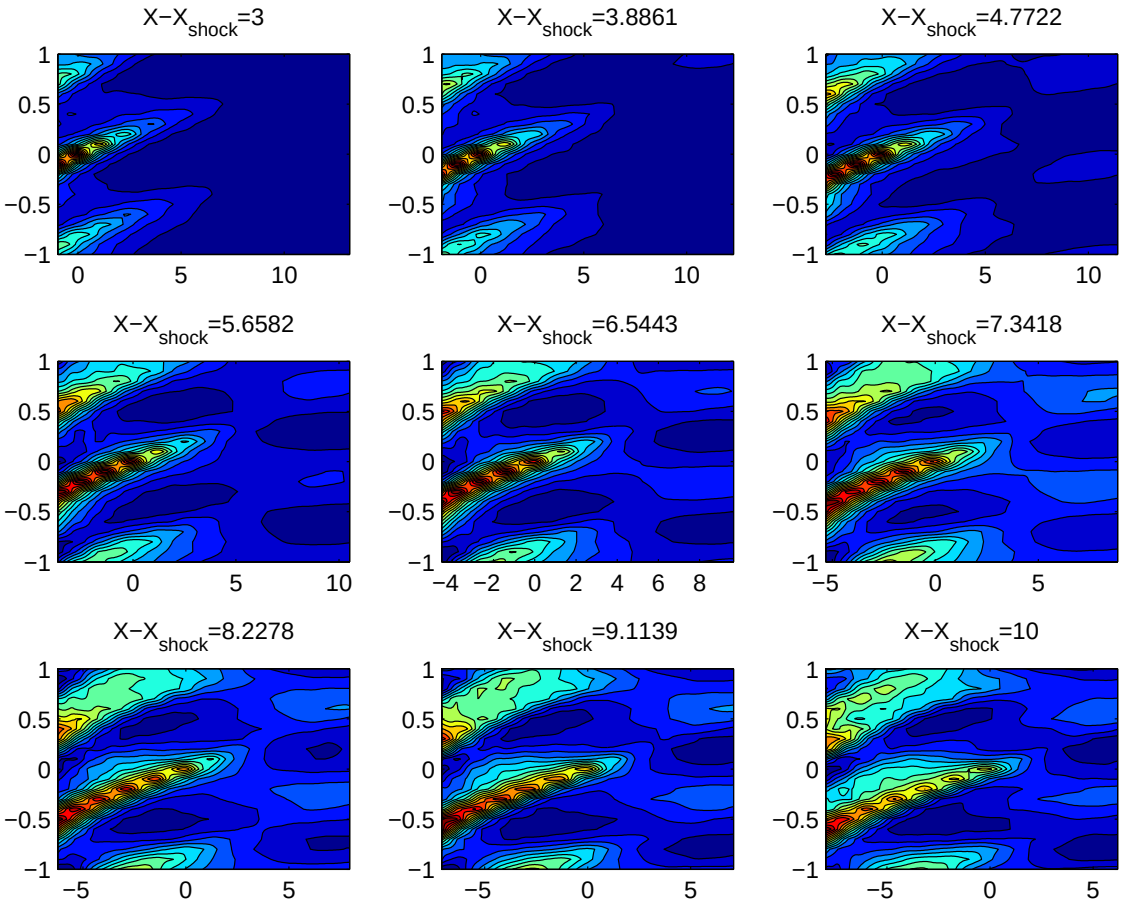

Figure 4. Similar layout as described in Fig. 2, but for entropy forced case.

III.A. Dynamic mode decomposition

DMD determines and ranks temporal evolution modes according to their coherency. The dynamic modes are the eigenvectors of a reduced evolution operator evaluated by algebraic manipulation of the matrix of solution snapshots. The extraction of modes does not involve spatial or temporal averaging, therefore, it overcomes the shortcomings of the bi-orthogonal[8] and proper orthogonal[8] analogs for the analysis of systems with a large spectrum of time and length scales (see discussion in Schmid[9]).

The reduced system dynamics is described by a low order matrix $\tilde{S}$ evaluated based on the matrix of snapshots $V_1^{n+1} \equiv \{v_1, v_2, \ldots, v_{n+1}\}$, where v_i is a column vector of size m representing the state of the system at an instant in time. The matrix $\tilde{S}$ is related to the full-system matrix A via an approximate similarity transformation $\tilde{S} = U^H A U$, where U contains the economy right singular vectors of $V_1^n = U \Sigma W^H$. The similarity transformation yields $\tilde{S} \equiv U^H V_2^{n+1} W \Sigma^{-1}$. In general, the size of the discretized system m is much larger than the number of snapshots n, thus the singular value decomposition is thin (see[10] p. 72) and the similarity transformation is approximate. The full-system eigenmodes are obtained by multiplying the right eigenvectors y_i (corresponding to the eigenvalues μ_i) of $\tilde{S}$ times U, i.e.,

$$\Phi_i = U y_i. \tag{3}$$

Each eigenmode is associated with a degree of coherence, $\chi_i = y_i^T \mathrm{Diag}\,(\Sigma)$, where $\mathrm{Diag}\,(\Sigma)$ is the economy size (i.e., length n) vector of singular values. The singular values rank the coherency of the time-averaged spatial structures, (i.e., the topos of[8]); the coherency of dynamic modes is, thus, evaluated as the product of the coherency of the topos and the coefficients of the linear mapping in equation (3).

The temporal modal frequencies $\lambda_i \equiv \log(\mu_i)$ are shown in Fig. 5 for the three cases. The vertical symmetry of the maps is explained by noting that λ values are either real or complex conjugate pairs, because $\tilde{S}$ is real by construction. The values are drawn with symbols of magnitude and color scale proportional to their coherency. Figure 5 shows a good degree of similarity between the maps of entropy-forced and non-forced cases, with a narrow distribution around the dominant real (large brown circle) eigenvalue. On the other hand, the vorticity-forced case features a wider distribution of eigenvalues, manifesting the presence of coherent short time scales. The coherence measure of the non-forced mode is markedly larger than that of the two forced analogs; moreover, vorticity supported structures are more coherent than the entropy analogs.

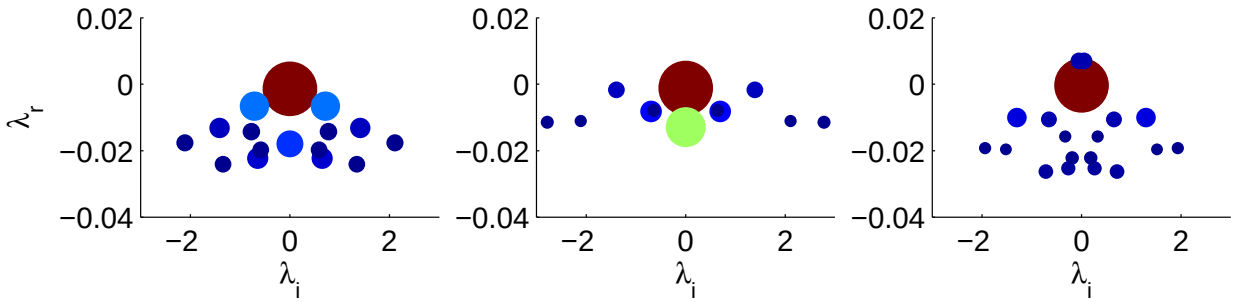

Figure 5. Maps of eigenfrequencies λ_i for non-forced (left), vorticity-forced (middle) and entropy-forced (right) detonations. The size and color of the symbols scales with the mode coherency.

The most coherent non-trivial eigenmodes, i.e., those with imaginary part different from zero, are shown in Fig. 6, where the first column refers to the non-forced case, the second to the vorticity-forced, and the third to the entropy-forced analog. Only the real parts of the dynamic mode of the mass fraction Y are shown. In fact, the imaginary parts are qualitatively similar to the real ones. The non-forced modes display the global motion of the triple-points; long range interaction can be inferred from the extension of the coherent regions; less coherent modes (2nd and 3rd panel of the first row) support fluctuations with a smaller spatial scale. The vorticity-forced case (second row) is dominated by a "stirring mode", which is not related to motion of the triple-point, but to the convected turbulence. The eigenvector features strongly coherent fluctuations in the post-shock, which promote mixing in the induction region. The second mode of the vorticity-forced case (second row and second column) is structurally similar to the second mode of the non-forced case (first row second column). The entropy-forced detonation is, also, dominated by a "stirring mode" featuring structures

elongated in direction parallel to the flow. Differently from the vorticity-forced case, the second global mode of the unforced case is not present. By examining the coherence measures reported on the title of each panel, we conclude that the entropy-forced case supports less coherent structures than the two other cases.

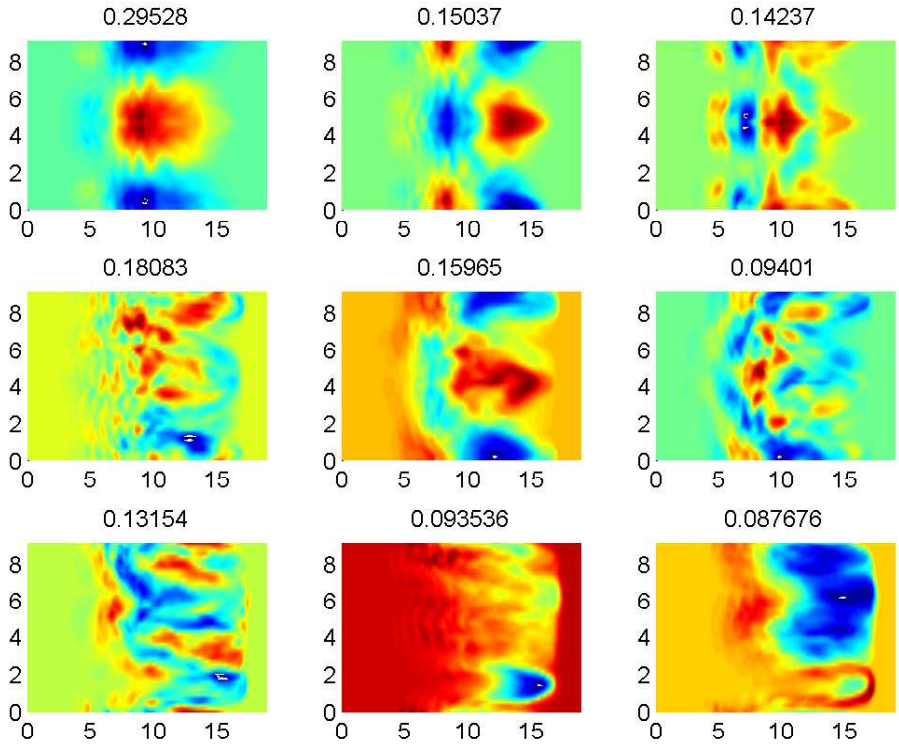

Figure 6. Most coherent modes in unforced (first row), vorticity forced (second row), and entropy-forced (third row) detonations. The title on top of each panel represent a measure of coherency, i.e., χ_i/χ_{max}. Note, the lefter-most panel has $\chi_i/\chi_{max} < 1$ because the most coherent mode is trivial, see Fig. 5.

IV. Conclusions

We present a computational analysis of Chapman-Joguet detonations with the goal of understanding the suitability of LES models based on the Taylor's hypothesis in the post-detonation regions. The analysis leads us to two main conclusions. First, the Taylor's hypothesis is not valid immediately behind the wave because of the contribution of evanescent pressure waves supported by the shock corrugation. Second, space-time correlations are not sufficient to distinguish the dynamic contribution of the interaction of turbulence and detonations. The averaging which is intrinsic in the evaluation of expected values in equation (1) leads to a loss of information. In this respect, we find that the dynamic mode decomposition of Schmid[9] performs much better in defining the contribution of convected and intrinsic detonation modes.

References

[1]Gelfand, B., Frolov, S., and Nettleton, M., "Gaseous detonations–A selective review," *Progress in energy and combustion science*, Vol. 17, No. 4, 1991, pp. 327–371.

[2]Massa, L. and Lu, F., "Role of the Induction Zone on Detonation-Turbulence Linear Interaction," *Combustion Theory and Modelling*, Vol. In press, 2011, pp. 10.1080/13647830.2010.540353.

[3]Massa, L., Chauhan, M., and F.K., L., "Detonation-turbulence interaction," *Combustion and Flame*, Vol. In press, 2011, pp. doi:10.1016/j.combustflame.2011.01.014.

[4]He, G., Wang, M., and Lele, S., "On the computation of space-time correlations by large-eddy simulation," *Physics of Fluids*, Vol. 16, 2004, pp. 3859.

[5]He, G. and Zhang, J., "Elliptic model for space-time correlations in turbulent shear flows," *Physical Review E*, Vol. 73, No. 5, 2006, pp. 055303.

[6]Morkovin, M., "Effects of compressibility on turbulent flows," *Mècanique de la Turbulence*, 1962, pp. 367–380.

[7]Baker, W., Cox, P., Westine, P., Kulesz, J., and Strehlow, R., *Explosion hazards and evaluation*, Elsevier Scientific Publishing Co., Amsterdam, The Netherlands, 1983.

[8]Aubry, N., Guyonnet, R., and Lima, R., "Spatiotemporal analysis of complex signals: theory and applications," *Journal of Statistical Physics*, Vol. 64, No. 3, 1991, pp. 683–739.

[9]Schmid, P., "Dynamic mode decomposition of numerical and experimental data," *Journal of Fluid Mechanics*, Vol. 656, 2010, pp. 5–28.

[10]Golub, G. and Van Loan, C., *Matrix computations*, Johns Hopkins Univ Pr, 1996.